Microwave volt-impedance spectroscopy of semiconductor structure

© A.N. Reznik, N.V. Vostokov

Institute for Physics of Microstructures, Russian Academy of Sciences,
603950 Nizhny Novgorod, Russia

E-mail: reznik@ipmras.ru

Received January 16, 2023
Revised March 2, 2023
Accepted April 25, 2023

Microwave voltage-impedance spectroscopy is used to study a semiconductor structure in the form of a doped *n*-GaAs film grown on a conducting n^+-GaAs substrate with a buffer sublayer. A system of concentric barrier contacts is formed on the structure surface. A technique has been developed for measuring complex impedance spectrum $Z(f, U)$ of the sample as a function of DC bias voltage U. Spectra $Z(f, U)$ were measured using a Cascade Microtech probe station in the frequency range $0.01-40$ GHz with a lateral resolution of $15-30\,\mu$m at $U = 0-10$ V. The main electrophysical characteristics of a semiconductor film were determined from the spectra: type, concentration and mobility of free charge carriers, electrical conductivity. An excess resistance was found in the range $f = 0.1-20$ GHz. This effect is interpreted as the deep states (traps) recharging for two types of traps — low-frequency l and high-frequency h with characteristic time $\tau_l = 10^{-9}$ s, $\tau_h = 4.2 \cdot 10^{-11}$ s. A model description is proposed that explains the characteristic shape of the trap resistance spectrum, its dependence on the contact area and voltage U.

Keywords: microwave band, near field, impedance, semiconductor, barier contact, deep states, electrophysical characteristics.

DOI: 10.21883/SC.2023.03.56232.4532

1. Introduction

Near-field microwave microscopy (NMM) — an effective tool for studying materials and structures at micro- and nanoscales [1–3]. Diagnostics of semiconductor materials and structures is currently considered as one of the most promising areas of application NMM [4]. The opportunity of obtaining quantitative information on some electrophysical characteristics of rather simple samples is demonstrated. In particular, the electrical conductivity of a bulk-homogeneous material, or the sheet resistance of a thin-film structure is managed to be determined with acceptable accuracy [5–14]. Meanwhile, the set of basic electrical characteristics of a semiconductor, which includes the type, concentration, and mobility of free charge carriers, even on scales of several tens of microns, cannot yet be determined using the NMM of classical designs. Existing diagnostic methods, as a rule, use some physical model that relates the measured electromagnetic response of the NMM to the desired characteristics of the object under study. The adjustable parameters of the models are determined from calibration measurements on reference samples. Due to the complex, often unknown geometric shape of the NMM probe, the accuracy of the corresponding models is insufficient for solving multiple-parameter inverse problems.

The transition to nanometer resolution is associated with additional difficulties. The point is that even volume-homogeneous semiconductors (unlike many other materials) on the nanoscale are complexly structured objects. Interaction with a metal probe and the presence of surface states lead to the fact that carrier-depleted/enriched area appears near the semiconductor surface, the thickness of which the thickness d of which is usually $\sim 50-200$ nm [15]. As a result, the inverse problem becomes multiple-parameter even in the simplest case of a homogeneous material. In addition, problems arise with the use of dielectrics and metals as reference samples for calibration. The use of semiconductor samples as standards is also difficult, since the parameters of the perturbed surface layer are difficult to control (besides the characteristics of the semiconductor, they also depend on the material, shape, and height $h \sim 10$ nm of the probe above the surface).

The formulated problem can be solved by a significant change in the design of NMM. In our studies [16,17] we used as a probe an antenna of a regular concentric shape, formed directly on the surface of a semiconductor. The diameter of the center disk of the antenna a determines the resolution. A constant voltage U is applied between the antenna electrodes, which allows to control the thickness $d(U)$ of the depleted near-surface layer. For microwave measurements of the electromagnetic response (frequency spectrum of the $Z(f, U)$ impedance of the probe-sample system), a commercial probe station is used. In the geometry under consideration, the dependence $d(U)$ is described by the classical theory of the Schottky contact [15]. In such a system, the probe model proposed in the paper [6] becomes suitable for solving minimum a three-parameter inverse problem. The known geometric characteristics of the antenna (diameter a and height $h = 0$) are „proper“ model parameters, so no additional measurements of adjustable parameters are required. In some cases, instead of a more general theory [6] rather simple analytical formulas

describing the equivalent scheme of the probe-sample system can be used. As a result, using a single-crystal GaAs substrate, the paper [17] demonstrated the possibility of determining the main electrophysical characteristics of a semiconductor (type of charge carriers, their concentration n and mobility μ, electrical conductivity σ, barrier band bending U_c) at $a = 10-60\,\mu$m. We called the corresponding diagnostic method proposed in the paper [18] microwave volt-impedance ($Z-V$) spectroscopy. In this paper $Z-V$-spectroscopy is applied to the study of a more complex film structure. The opportunity of determining the electrical parameters of a semiconductor film under conditions where the traditional four-probe method (DC Hall measurements in Van der Pauw (VDP) geometry) does not allow to determine the indicated parameters is shown.

Another result of the paper [17] (more detailed in the article [19]) was the study of non-trivial resistive properties of the Schottky contact. „Excess resistance" found in the frequency range $f = 10-300$ MHz was associated with the recharging of deep states (traps) present in the semiconductor. Standard methods of trap investigation (admittance spectroscopy and non-stationary deep-level spectroscopy) are performed with a temperature pass (often from helium) in the lower frequency band and do not provide locality $\sim 10\,\mu$m. Microwave $Z-V$ spectroscopy allows to determine the concentration of traps at room temperature with micron resolution. The high-frequency (up to 67 GHz) measurements carried out in this paper allowed to detect atypical states (presumably traps) with an extremely fast ($\sim 4 \cdot 10^{-11}$ s) recharge time in the studied sample.

2. Measurement technique and studied sample

We have studied a homogeneous in the lateral plane semiconductor structure, which was a sulfur-doped (S) n-GaAs film and an n^+-GaAs sublayer with a thickness of $d_1 = 1\,\mu$m and $d_2 = 1.5\,\mu$m, respectively (see Fig. 1). The structure was grown on a conducting GaAs substrate. Layer thicknesses and dopant concentration N_S were determined by secondary ion mass spectrometry (SIMS). According to these data, the depth profile of the concentration S in relative units has the form shown in Fig. 2. The electrical conductivity of the substrate $\sigma_s = 500\,(\text{Ohm} \cdot \text{cm})^{-1}$ was measured by the VDP method. A system of concentric barrier contacts (antenna system) was formed over the structure. Each 1.5×1.5 mm block of the system was a lattice of nine antennas. One of the unit antennas is schematically shown in Fig. 1. The technology for contacts deposition is described in [17]. In microwave measurements, we used two antennas A1, A2 with a diameter of the central contact $a = 14$ and $27\,\mu$m. Internal diameter of external contact $b = 57\,\mu$m (A1), $68\,\mu$m (A2) at $c = 0.5$ mm. Scale a determines the lateral resolution of the $Z-V$ method. The issue of resolution is discussed in detail at the end of Section 3. In a semiconductor film

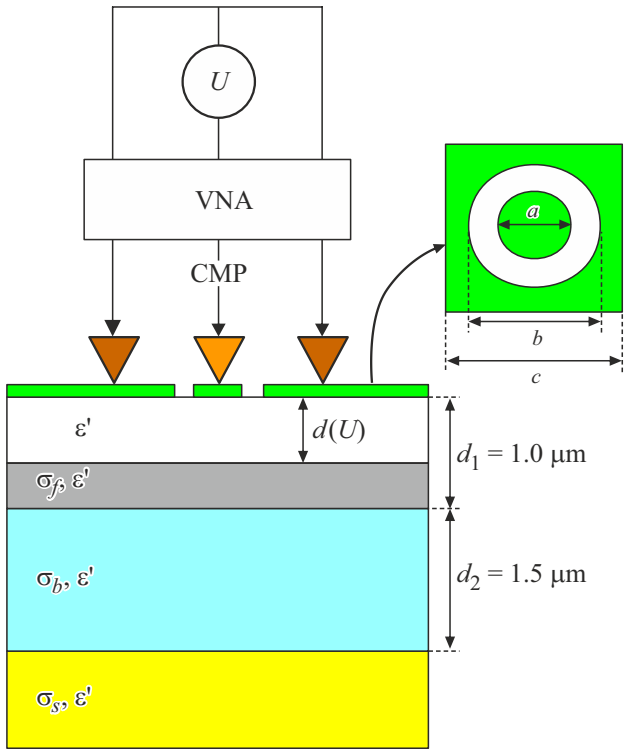

Figure 1. Scheme of measurements and structure under study. VNA — vector network analyzer. CMP — CM probe. On the insert — view of the concentric antenna from above.

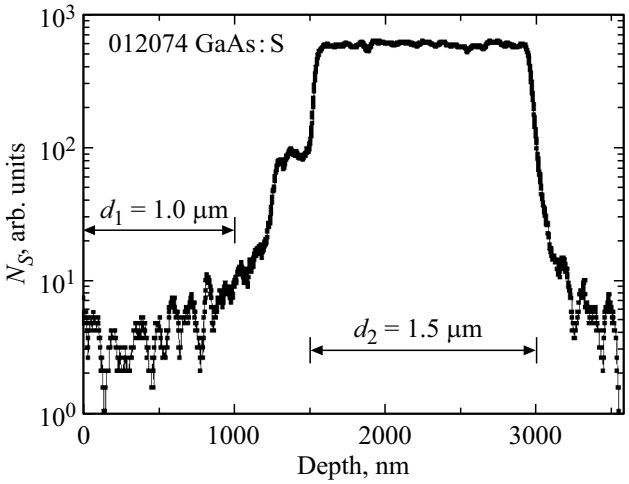

Figure 2. Impurity concentration profile (S) according to SIMS data.

near to the interface with metal, a flat deplated layer is formed. The thickness of layer is $d(U)$ ($d \ll a$), where U — constant voltage applied between the central and external contacts of the antenna.

The spectrum of the complex reflectance $\Gamma(f, U)$ of the structure was measured using a Cascade Microtech (CM) commercial probe station. The CM probe in the form of a symmetric coplanar line with a coaxial junction was

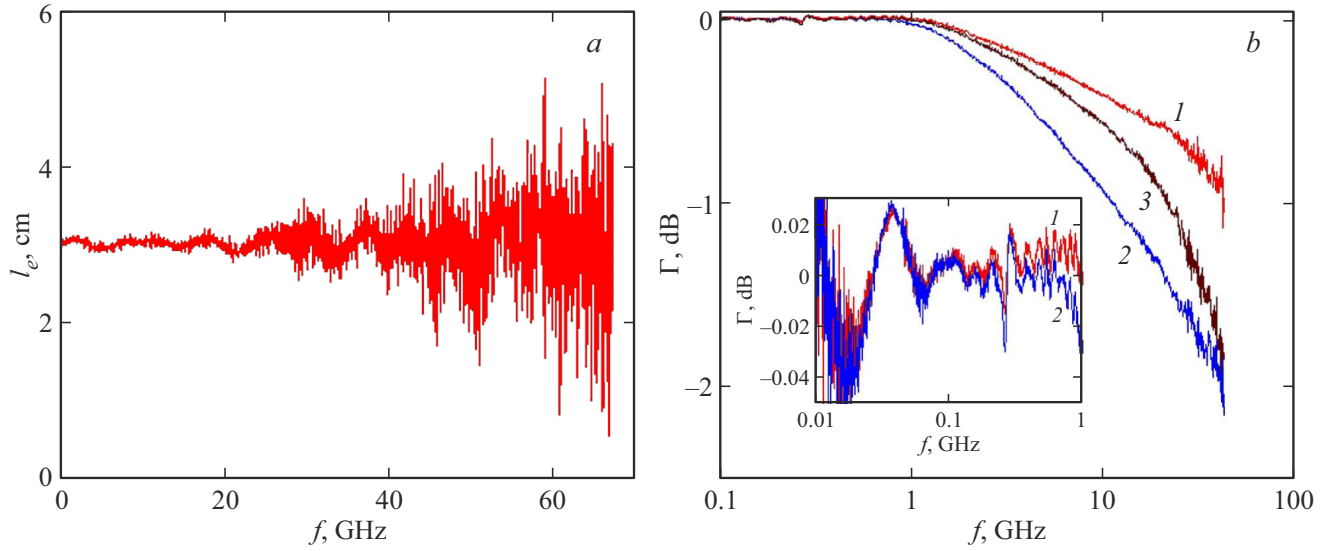

Figure 3. *a* — spectrum of the electric length of the CM probe from measurements in the Air mode. *b* — reflectance spectrum $|\Gamma(f)|$ of CM probe: *1* — Air; *2, 3* — antenna A2 at $U = 0$, 10 V respectively. On the insert — the low-frequency part of the spectrum $|\Gamma(f)|$: *1* — Air, *2* — antenna A2 at $U = 0$.

connected to an Agilent E8361 A vector network analyzer (VNA) and brought into contact with one of the antennas in the sentral part of the sample (see Fig. 1). A single-port calibration of the VNA was preliminarily carried out using a standard electronic device connected to a coaxial cable, which was used to connect the VNA to the CM probe. The voltage $U = 0, 1, 2, \ldots, 10$ V was supplied from an external source through a circuit decoupled from the microwave path. Microwave measurements were performed in the frequency range $f = 0.01-67$ GHz (1600 points on a logarithmic scale). Let us note that the measuring system allows performing diagnostics at different points of the structure surface, passing from block to block of the antenna system, as was done in the paper [16]. In this paper, we dealt with a laterally homogeneous structure, so the measurements were carried out in one antenna block.

From the measurements of the $\Gamma(f, U)$ spectrum, we determined the complex impedance spectrum of the CM probe — test sample system $Z(f, U) = R(f, U) - iX(f, U)$. The measurement technique was as follows. CM probe was modeled by a homogeneous two-wire line of length l with wave impedance Z_{CM} and wave vector $k_{\text{CM}} = (2\pi f\sqrt{\varepsilon_l'}/c)(1 + i\delta)$, where c — speed of light, ε_l' — dielectric constant of the line. We assume $Z_{\text{CM}} = Z_0 = 50$ Ohm, where Z_0 — is the impedance of the coaxial cable connecting the CM probe to the VNA. The electrodynamics of the modeling CM probe line is completely characterized by two parameters — electric length $l_e = \sqrt{\varepsilon_l'}l$ and attenuation δ. These parameters were determined in the set of calibration measurements in the absence of contact between the CM probe and the test sample (Air mode). The l_e length is determined by measuring the $\varphi(f)$ phase spectrum of the $\Gamma(f)$ factor in Air mode. For an end-open line, the VNA clamped phase is defined as $\varphi(f) = (4\pi f/c)l_e$. Then the length measured in centimeters is $l_e(f) = \Delta\varphi(f)/(24\Delta f)$, where $\Delta f = f_2 - f_1$, $\Delta\varphi = \varphi(f_2) - \varphi(f_1)$ — phase difference in degrees according to measurements at two frequencies $f_{1,2}$ in GHz, and $\Delta f \ll f = (f_1 + f_2)/2$. Spectrum $l_e(f)$ is shown in Fig. 3, *a*. It can be seen that the length l_e does not depend on f, and the average value of $l_e = 3.02$ cm in the entire spectral interval. In the $f < 20$ GHz range, the phase is measured quite accurately, so that the accuracy of determining l_e turns out to be no worse than a few percent. At higher frequencies in the VNA operating mode used, the accuracy of the $\varphi(f)$ spectrum measurements decreases. As a result, we get the lenth l_e jumps from point to point, reaching 50–100% (from 1.5 to 4.5 cm) at $f > 60$ GHz (see Fig. 3, *a*). In this regard, the $Z(f)$ spectrum was determined in a narrower range $f \le 40$ GHz, where the value l_e was assumed to be equal to the average value with acceptable accuracy. As will become clear from what follows, the specified limitation of the range does not prevent the solution of the problems posed in this work.

The next calibration step was to determine the spectrum of the loss factor $\delta(f)$ in the CM probe modelling line. For this purpose, the following ratios were used for the reflectance Γ:

$$\Gamma(f, \delta) = \frac{Z_{\text{in}}(f, \delta) - Z_0}{Z_{\text{in}}(f, \delta) + Z_0}, \tag{1}$$

$$Z_{\text{in}}(f, \delta) = Z_{\text{CM}}\frac{Z + iZ_{\text{CM}}\,\text{tg}\big(k_{\text{CM}}(f, \delta)l\big)}{iZ\,\text{tg}\big(k_{\text{CM}}(f, \delta)l\big) + Z_{\text{CM}}}, \tag{2}$$

where $k_{\text{CM}}l = (2\pi f l_e/c)(1 + i\delta)$. In formula (2) in Air mode, the line load impedance is $Z = -i\infty$. The $\delta(f)$

spectrum was found by solving the equation:

$$|\Gamma_e(f)| = |\Gamma(f, \delta)|, \tag{3}$$

on the left side of which is the experimental spectrum of the reflectance obtained during the calibration (curve *1* in Fig. 3, *b*), on the right side — the spectrum calculated by the formulas (1), (2). Thus, as a result of the calibration, the line parameters necessary for measuring Z were determined — length l_e and spectrum $\delta(f)$.

The $R(f)$ spectra obtained below are reliable in the $f > 0.1$ GHz range, since here the reflectance on the sample is $|\Gamma_s(f|) < |\Gamma_{\text{air}}(f)|$, which can be seen from Fig. 3, *b* and in the insert to this figure. This inequality means that when the probe contacts the sample, additional losses arise due to the fact that the load impedance in formula (2) contains the real part $\text{Re}(Z) = R \neq 0$. Considering the above, the frequency range in which the $R(f, U)$ spectra were determined is narrowed to $0.1\,\text{GHz} < f < 40\,\text{GHz}$.

To determine the $Z(f, U)$ impedance spectrum, the $\Gamma_e(f, U)$ spectrum was measured at the contact of the SM probe with A1, A2 antennas on the sample surface. Spectra $X(f, U)$, $R(f, U)$ for each value U are obtained by solving the system of equations:

$$\Delta\varphi_e(f, U) = \Delta\varphi_t(f, X, R), \tag{4a}$$

$$|\Gamma_e(f, U)| = |\Gamma_t(f, X, R)|. \tag{4b}$$

The phase of the reflectance in degrees is calculated as

$$\varphi_t(f, X, R) = \text{arctg}\left[\frac{\text{Im}\big(\Gamma_t(f, X, R)\big)}{\text{Re}\big(\Gamma_t(f, X, R)\big)}\right]\frac{180}{\pi}. \tag{5}$$

The theoretical spectrum of $\Gamma_t(f)$ in (4), (5) was calculated by formulas (1), (2), where the sample impedance is the desired function of $Z(f, U) = R(f, U) - iX(f, U)$, and the line parameters l_e, δ are determined during calibration. The experimental and calculated phase shift on the sample in (4a) are taken relative to the calibration values for each frequency f. Meanwhile, for $\Delta\varphi_e$, the difference between the experimental spectra on the sample and in the Air mode — $\Delta\varphi_e = \varphi_e^s - \varphi_e^{\text{Air}}$ is taken. In the calculation of the function $\Delta\varphi_t(f, X, R)$ (the right side of the equation (4a)), the function is taken as the calibration value for phase of the coefficient $\varphi_t^{\text{Air}}(f, X = -i\infty, R = 0)$ in (1), (2).

The solution of the system of equations (4) with respect to the parameters X, R was carried out using the Given−Find(X, R) subroutine of the commercial Mathcad package, which caused some technical problems. The point is that the phase measured by the VNA is fixed in the range $-180 < \varphi_e < +180°$, and the calculation of the phase by formula (5) gives $-90 < \varphi_t < +90°$. As a result, jumps are observed in the spectra of $\varphi_{e,t}(f)$ at the transition of boundary values, as a result of which the phase differences of $\Delta\varphi_{e,t}$ are calculated incorrectly in some cases. The problem is quite easily eliminated by software for the experimental spectra $\varphi_e^s(f)$, $\varphi_e^{\text{Air}}(f)$ and in the theoretical spectrum $\varphi_t^{\text{Air}}(f)$, after which the corresponding functions become continuous over the entire range f. For the function $\varphi_t^s(f, X, R)$, calculated inside the Given−Find subroutine, phase jumps are not eliminated, which is why the system of equations (4) has no solution in the entire considered frequency range. The way out is to split the f range into $m_{\max}$ separate sectors of length $\Delta f_m \approx 2.4$ GHz, in which the $\varphi_t^s(f, X, R)$ function is continuous. In each m interval we get a different number of discrete phase values M_m in the logarithmic frequency scale. At transition from sector to sector, the number $180m$ $(m = 1, 2, \ldots, m_{\max})$ is added to the right side of equation (4a). For each computed spectrum, the boundaries of the sectors are selected empirically from the condition for the existence of a solution in the entire sector. To obtain the final spectra $X(f, U)$, $R(f, U)$ all sectors are stitched together. As the frequency f increases, the number of M_m decreases. For example, for an antenna A2 at $U = 0$ in the range $0.01\,\text{GHz} < f < 40\,\text{GHz}$ we have $m_{\max} = 17$, and $M_1 = 996, \ldots, M_5 = 40, \ldots, M_{16} = 12 \ldots$. Thus, the process of obtaining $Z(f, U)$ spectra turns out to be quite laborious, and the limitation of the range by the maximum frequency $f = 40$ GHz is another argument from the point of view of reducing the time spent on processing experimental data.

3. Impedance spectra

The reconstructed spectra of reactance $X(f)$ and resistance $R(f)$ of the probe in contact with the sample are shown in Fig. 4 for antennas A1, A2 at $U = 0, 2, 10$ V. The reactance spectrum of $X(f, U)$ is related to the thickness of the depleted layer $d(U)$ by the relation (justification see Sec. 4):

$$X(f, U) = \frac{1}{2\pi f C_d(U)}, \tag{6}$$

where the capacitance

$$C_d(U) = \frac{\varepsilon'\varepsilon_0 S_a}{d(U)}, \tag{7}$$

ε_0 — vacuum electric constant, $\varepsilon' = 12.9$ — permittivity of GaAs. Formulas (6), (7) allow to determine the dependence $d(U)$ from measurements of the spectrum $X(f, U)$. The corresponding results for antennas A1, A2 are shown in Fig. 5 in the normalized variables $u = 1 + U/U_c$, $v = (d/d_0)^2$. The obtained $d(U)$ function corresponds to the following parameter values: $d_0 = 175$ nm, $U_c = 0.885$ V, for which the experimental points in Fig. 5 lie with the least square deviations on the line $v = u$, which corresponds to the classical depletion theory [15] (complete depletion approximation). The type of free charge carriers in the film is determined by the sign of the bias voltage at the central electrode of the antenna. In our case, the function $d(U)$ grows with the growth of U at a negative bias, which corresponds to carriers of the *n*-type. At $U \leq 10$ V, the maximum value d did not exceed 600 nm,

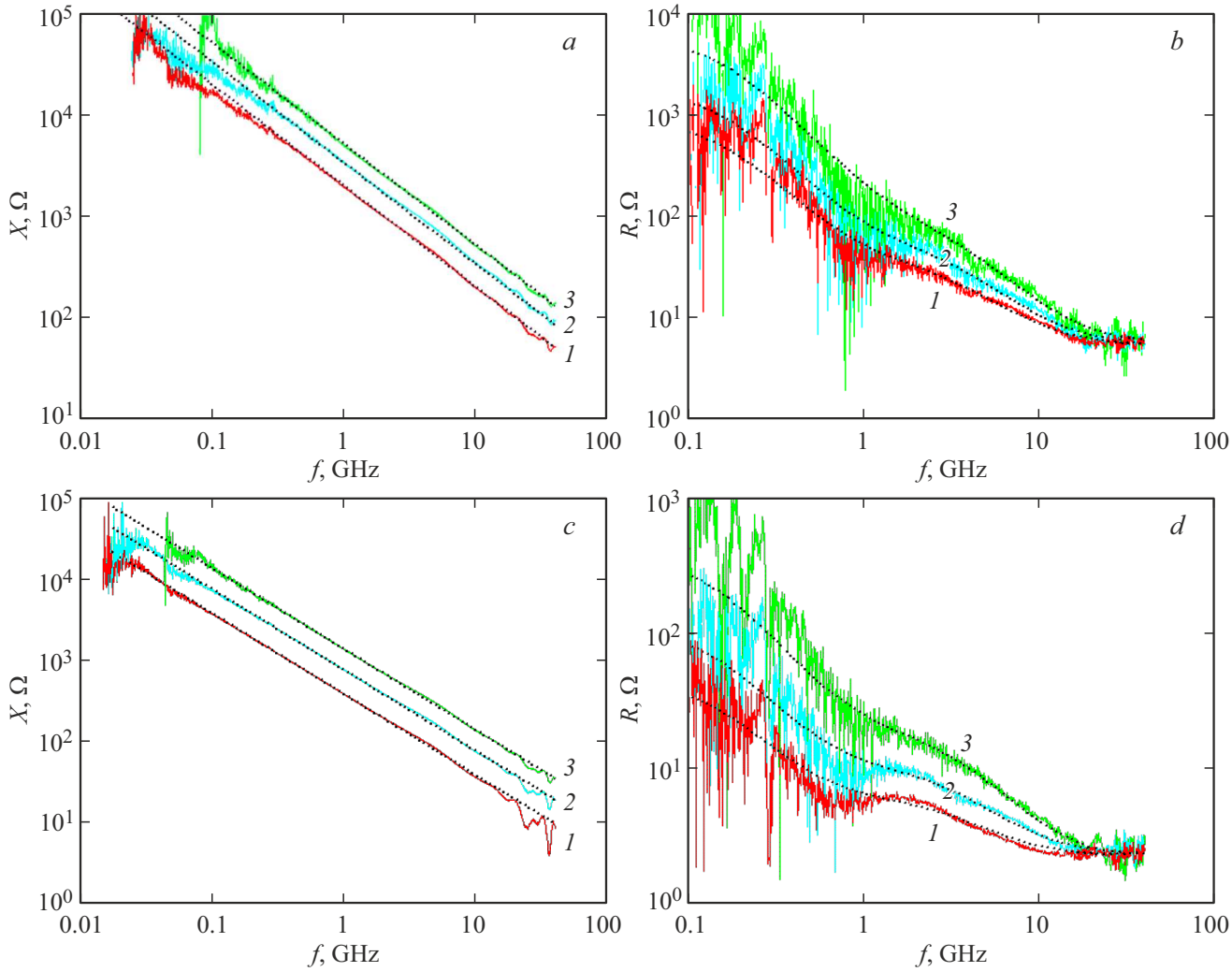

Figure 4. Spectrum of reactance (a, c) and resistance (b, d) of antennas A1 (a, b), A2 (c, d) for $U = 0$ (1), 2 (2), 10 V (3). Solid lines — experimental data, dashed lines — calculation results.

which is less than the film thickness d_1. As a result, it turned out to be possible to determine the electron concentration in the film n_f, but not in the buffer layer and substrate. According to the depletion theory, we have $n_f = 2\varepsilon'\varepsilon_0 U_c/(ed_0^2) = 4.1 \cdot 10^{16}\,\mathrm{cm}^{-3}$, where e — charge of an electron. Theoretical reactance spectra in Fig. 4, a and c were calculated by formulas (6), (7) taking into account the obtained dependence $d(U)$. We can state a good agreement between the experimental and theoretical spectra $X(f, U)$.

The $R(f, U) = \mathrm{Re}\big(Z(f, U)\big)$ spectra shown in Fig. 4, b and d demonstrate excess resistance in the range 0.1–20 GHz, which we also found in [17] and studied in [19] for single-crystal GaAs substrate. If, as in [19], we assume that this resistance is due to the recharging of deep states (traps), then the sample under consideration contains two types of traps — low-frequency (l) and high-frequency (h) with characteristic recharging time $\tau_l \gg \tau_h$. The next section shows that the $R(f, U)$ spectrum can be represented as

$$R(f, U) = R_l(f, U) + R_h(f, U) + r(f). \qquad (8)$$

In formula (8), the depletion layer resistance $R_l + R_h$, associated with the recharging of h- and l-traps, determines the above-mentioned excess resistance, which is not taken into account by the elementary theory of the Schottky contact [20]. The resistance of traps of a certain type $t \to l, h$ is described by a formula, which derivation is also given in the following section:

$$R_t(\omega, U) = R_s^t \chi_t(U)\,\frac{1}{1 + \omega^2\tau_t^2}, \qquad (9)$$

where $\omega = 2\pi f$, R_s^t — saturation resistance $(R_t(\omega, U{=}0) \to R_s^t$ at $\omega\tau_t \ll 1)$, $R_s^t S_a = \rho_t = (\tau_t/c_0)(n_t/n_f)$, $c_0 = \varepsilon_0\varepsilon'/d_0 = 6.5 \cdot 10^{-4}\,\mathrm{F/m}^2$, $S_a = \pi a^2/4$ — the area of the central contact of the antenna, n_t — concentration of

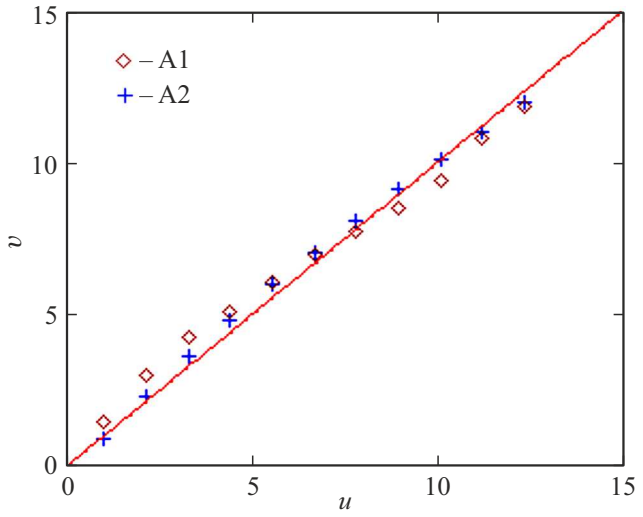

Figure 5. Dependence of $d(U)$ in normalized variables for antennas A1 and A2. Icons — experimental data, solid line — $v = u$ function.

trap charge carriers. Function

$$\chi_t(U) = \sqrt{1 + U/U_c} \tag{10}$$

characterizes the dependence of the resistance R_t on the voltage U. The problem of the model description of the resistance of traps is reduced to finding the parameters τ_t, ρ_t from the experimental data, from which the concentration n_t is determined. The resistance $r(f)$ in formula (8) is determined by the unperturbed region of the semiconductor structure and consists of three components — resistance r_f of the part of the semiconductor film located under the depletion layer, the buffer layer r_b and the substrate r_s, i.e.

$$r(f, U) = r_f(U) + r_b + r_s(f). \tag{11}$$

When the ratio of film and buffer layer thicknesses is $d_{1,2} \ll a$, the microwave current flows orthogonally to the corresponding layers of the structure under study. In this case we have

$$r_f(U) = \frac{d_1 - d(U)}{\sigma_f S_a}, \tag{12a}$$

$$r_b = \frac{d_2}{\sigma_b S_a}, \tag{12b}$$

where σ_f, σ_s — conductivity of the film and buffer layer, $d(U) < d_1$. The substrate thickness $d_s = 0.35\,\text{mm}$ is inversely related to the antenna diameter $d_s \gg a$, that is why the current spreading in the substrate has a three-dimensional structure. Under these conditions, the resistance of the substrate will be characterized by the relation [21]

$$r_s(f) = \frac{1}{2\pi}\left[\sqrt{\frac{\omega\mu_0}{2\sigma_s}}\ln\left(\frac{b}{a}\right) + \frac{2}{\sigma_s a}\operatorname{arctg}\left(\frac{b}{a}\right)\right], \tag{13}$$

where μ_0 — permeability of vacuum. Taking into account the value of σ_f obtained in further studies, the ratio of dopant concentrations in the film and buffer layer $N_b/N_f \sim 10^2$ (see Fig. 2), and the substrate conductivity $\sigma_s = 500\,(\text{Ohm}\cdot\text{cm})^{-1}$ found from the data of VDP measurements, we arrive to the hierarchy of resistances $r_f \gg r_s \gg r_b$. In this situation, we will neglect the contribution of the buffer layer resistance to (11).

Taking into account the asymptotics of the resistance spectrum of traps (9) $R_t(f) \sim (\omega\tau_t)^{-2}$ at $\omega\tau_t \gg 1$ and the saturation of these functions at $\omega\tau_t \ll 1$, we can conclude that each term of the formula (8) dominates in different frequency areas — 0.1–1; 1–10; 10–40 GHz for R_l, R_h, r respectively (see Fig. 4, *b* and *d*). This allows to estimate the parameters of the function (9) for *l*-, *h*-traps without solving a multi-parameter inverse problem. We have the values of the parameters of the function (9) averaged over all data for *l*-, *h*-traps: $\tau_l = 10^{-9}\,\text{s}$, $\rho_l = 8\cdot10^{-4}\,\text{Ohm}\cdot\text{cm}^2$, $n_l/n_f = 5.2\cdot10^{-2}$; $\tau_h = 4.2\cdot10^{-11}\,\text{s}$, $\rho_h = 3.1\cdot10^{-5}\,\text{Ohm}\cdot\text{cm}^2$, $n_h/n_f = 4.8\cdot10^{-2}$. Note, the *l*-traps parameters can only be estimated in order of magnitude, since in the obtained spectra of $R(f)$ there are no reliable data on the resistance in the range $f < 0.1\,\text{GHz}$, but at frequencies 0.1–1 GHz, where *l*-traps make a dominant contribution to the resistance, the spectra of $R(f)$ in Fig. 4, *b, d* are strongly noisy. The reasons for the increased noises are discussed in detail in the paper [19], where a resonance spectroscopy method has also been developed, which allows to reduce these noises. Measurements by this method will provide the necessary data for a more accurate determination of *l*-traps parameters.

The $\chi_t(U)$ function is shown in Fig. 6 along with experimental data for *l*-, *h*-traps. It can be seen that formula (10) satisfactorily describes the experimental dependences for *h*-traps, while for *l*-traps there is a significant discrepancy between this formula and experiment. This discrepancy can be explained by the above inaccuracy in measuring the $R_l(f, U)$ spectra. Another reason may be related to the inhomogeneity of the depth profile of the $n_l(z)$ concentration. Obviously, the growth of n_l with depth will lead to a steeper dependence of $\chi_t(U)$ compared to the function (10). In this case, the obtained estimate n_l corresponds to the depth $z = d_0 = 175\,\text{nm}$. At a depth of $z = d(U = 10\,\text{V}) \approx 600\,\text{nm}$, the concentration n_l can increase in ~ 2 times.

In the high frequency region $f > 10\,\text{GHz}$, the resistance of the structure under study is determined mainly by the unperturbed region of the semiconductor and the substrate $r(f, U) = r_f(U) + r_s(f)$, where the resistances $r_{f,s}$ are calculated by formulas (12a), (13). Nevertheless resistance $R_h(f, U)$, described by formula (9) with the above parameters of *h*-traps makes a significant contribution to the spectrum $R(f, U)$ at these frequencies, which can be seen from Fig. 4, *b, d*. For the conductivity of the substrate $\sigma_s = 500\,(\text{Ohm}\cdot\text{cm})^{-1}$ found from VDP measurements, we obtain the average value of the conductivity of the semiconductor film $\sigma_f = 8.1 \pm 1.1\,(\text{Ohm}\cdot\text{cm})^{-1}$ over all spectra. Taking into account the above value n_f, we

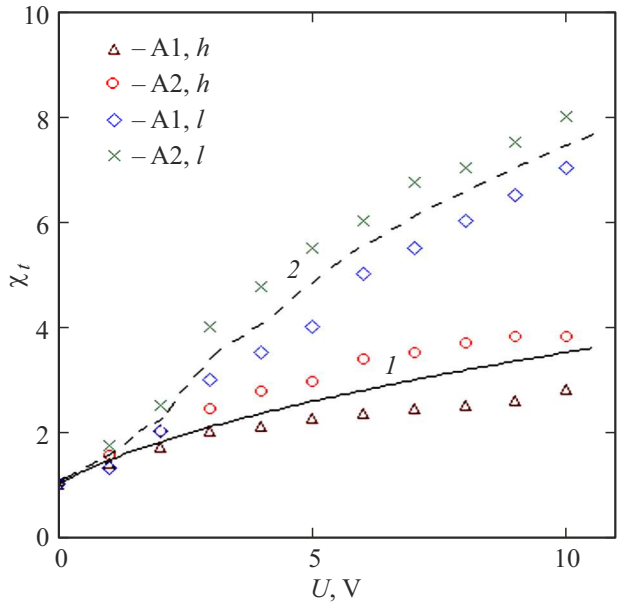

Figure 6. Dependence of resistance of l-, h-traps on voltage U by measurements of antennas A1, A2 — icons. Curve *1* — calculation by formula (10), *2* — empirical function.

find the mobility of electrons in the semiconductor film $\mu_f = \sigma_f/(en_f) = 1.2 \cdot 10^3\,\mathrm{cm}^2/(\mathrm{V}\cdot\mathrm{s})$. Let us note that, due to the relation $r_f \gg r_s(f)$, the frequency dependence of the resistance $r(f)$ in (11) is rather weakly expressed. This is despite the fact, that the skin layer depth in the substrate $\delta_{sk} = \left(2/(\omega\sigma_s\mu_0)\right)^{1/2} \sim a$ in the range $f = 20{-}40\,\mathrm{GHz}$, so that the first term of the formula (13) corresponds in order of magnitude to the second. As a result, at $f > 20\,\mathrm{GHz}$ we have $R(f) \approx \mathrm{const}$, and the dependence $R(f)$ at $f < 10\,\mathrm{GHz}$ is determined by the resistance of the traps $R_{l,h}(f, U)$.

Let us pay attention to the fact that VDP diagnostics of the structure under study does not allow to determine the electrophysical parameters of the film due to the shunting effect of the substrate. Indeed, in four-probe VDP measurements at direct current, there is a parallel connection of the resistances of the substrate R_s and the film r_f, as a result of which, at $d_s = 0.35\,\mathrm{mm}$, the total resistance is $R \approx R_s \approx 1/(\sigma_s d_s) \ll r_f$. In our geometry of microwave $Z{-}V$-spectrometry, the reverse situation is realized — series connection of resistances r_f and r_s. That is why we obtain $r \approx r_f \gg r_s$, which allowed us to determine the conductivity σ_f of a semiconductor film. A serious factor that makes it difficult to determine the resistance r of the unperturbed area of the sample is due to high-frequency traps. Presence of such traps and the associated excess resistance R_h at high frequencies ($f > 3\,\mathrm{GHz}$) qualitatively distinguishes this sample from the previously studied GaAs substrate [17,19]. Nevertheless, we managed to determine the r resistance by introducing a model function (9) describing the resistance $R_h(f, U)$ of the h-traps. This allowed to obtain quite reasonable values for the σ_f, μ_f parameters in these difficult conditions.

The results of calculating the resistance spectra $R(f, U)$ by formulas (8)–(13) for antennas A1, A2 using the above model parameters are shown in Fig. 4, *b, d* by dashed lines. When calculating the spectrum $R_h(f, U)$ (9), the function $\chi_t(U)$ (10) (curve *1* in Fig. 6) was used, for the spectrum $R_l(f, U)$ — the empirical function (curve *2* in Fig. 6). It can be stated that the calculations agree satisfactorily with the experimental data. Function (9) describes quite well the shape of the frequency spectra $R_{l,h}(f)$, as well as their dependence on the diameter a of antennas at $U = 0$. Taking into account the analysis of literature data performed in the next section, as well as the existing discrepancies with experiment for the dependence of the $R_l(f)$ spectra on the voltage U, the $\chi_t(U)$ function requires a more thorough study. On the whole, the data obtained support the proposed interpretation of the observed excess resistance as additional microwave losses for traps recharging.

Let us consider in more detail the question of the lateral resolution of the $Z{-}V$ method. In the paper [6], a quasi-static model for the coaxial antenna impedance is developed, taking into account both the internal a and external b, c scales in Fig. 1. It was assumed that external sources are concentrated only on the metal surfaces of the antenna, and outside these surfaces are absent. The calculation according to the model showed that for the structure with the obtained parameter values, the influence of the external contact on the antenna impedance does not exceed a few percent. The equivalent scheme of the probe-sample system, which takes into account the external contact, is given in [16]. Due to the ratio of the areas of the central and external contacts $S_a \ll S_{bc}$, we can assume the impedance of the external circuit of this scheme $Z_{bc} \to 0$ (short circuit). These circumstances are reflected in the relations (7), (9), (12), according to which the components of the antenna impedance are determined only by the diameter of the central contact a. This means that at sounding depths $z \le d_1$ the resolution is equal to the diameter a (see also [16]). It should be noted that this conclusion only applies to $z \ll a$ depths. Potentially, the $Z{-}V$ method works at greater depths $z \sim a$. In our case, the appropriate diagnostics would make it possible to determine the conductivity of the substrate σ_s. However, for the test sample, due to the above ratio $r_s \ll r_f$, the accuracy of such diagnostics turned out to be low. The solution of the inverse problem with respect to σ_s using different sets of experimental data obtained for different frequencies f, voltages U and diameters a demonstrated variations in the values of σ_s by more than 50% relative to the value found from the VDP measurements. In this regard, we limited ourselves to solving a narrower problem of determining the electrical parameters of the film using VDP data for σ_s. The foregoing does not remove the issue of estimating the resolution at depths $z \sim a$, which obviously deteriorates with increasing z. The latter can be seen from the formula (13), according to which

the influence of the outer scale of the antenna b on the resistance r_s is quite noticeable. The resolving power of near-field microscopes was studied in [12,22–25]. It is shown that the resolution is determined by the effective diameter of the probe aperture a. The most consistent analysis of the lateral resolution of the probe is performed by scanning an artificial contrast object embedded in the medium under study. In this case, the linear size of the object is $\rho_0 \ll a$, but the contrast of its permittivity should provide a noticeable change in the probe impedance for the microscope (spectrometer). In our implementation of the $Z-V$ method, the sample is not scanned, which virtually excludes the opportunity of a corresponding experimental study. The theoretical analysis of the problem is possible on the basis of solving the problem of diffraction of the quasi-static field of the probe on a three-dimensional object. For some model of a microscope probe and a spherical object, a such solution was obtained in the paper [26]. The sensitivity area of the probe was calculated in a plane located at a distance of z from the aperture. This area grows with an increase in z and at $z \sim a$ it can 2–3 times exceed the aperture area S_a depending on the permittivity ε of the medium in which the spherical object is embedded. A similar analysis can be performed for the coaxial antenna and multilayer medium considered here, which requires a separate study.

4. Deep states

Formulas (6), (8), (9) for the impedance of a structure with a barrier contact containing traps require explanation. A large number of papers have been devoted to the study of such structures, starting from the 50s years. In the papers [27–30], simple analytical expressions for the impedance are obtained, based on a number of fairly general simplifying approximations. Let's perform the analysis based on the results of the paper [28], where an equivalent cirquit of the structure with an arbitrary number of deep states is proposed. The energy diagram for the two-state case under consideration is shown in Fig. 7. The calculation of the energy of the bottom of the conduction band $E_c(x)$ was performed at $U = 1$ V in the full depletion [15] approximation, when $d = d_0\sqrt{1+U/U_c}$. It was assumed that in the quasi-neutral region of $x < 0$, all dopant atoms are ionized, and deep levels are completely filled. In the depleted area $0 < x < d$ on the $x = x_{l,h}$ planes, the energy of deep states $E_t(x)$ becomes equal to the Fermi energy E_F. In the absence of a variable field, the corresponding deep levels are empty at $x_{l,h} < x < d$ and filled at $x < x_{l,h}$. In the quasi-neutral region, the trap level depth is $\Delta_{l,h} \gg E_c - E_F$ and on the scale of Fig. 7 for $x < 0$ we have $E_c \approx E_F$.

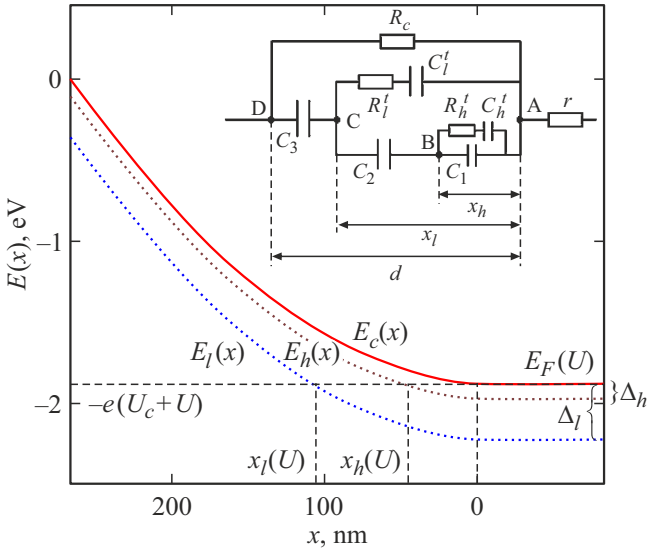

Figure 7. Energy level diagram. Dashed lines — energy levels of deep states. On the insert — the equivalent scheme of the structure according to [28].

Under the action of an alternating voltage, the Fermi level oscillates. Meanwhile, in a narrow region (~ 10 nm) near the coordinates of the $x = x_{l,h}$ planes, the traps are recharged, which changes the complex impedance of the entire system. In the equivalent scheme (see inset in Fig. 7), the indicated effect is described by additional impedances $Z^t_{l,h} = R^t_{l,h} - i/\omega C^t_{l,h}$ (series connection of the corresponding capacitances and resistances), and the characteristic recharge time is $\tau_{l,h} = R^t_{l,h} C^t_{l,h}$. Scheme elements are expressed as

$$C^t_{h,l} = \tau_{l,h}/R^t_{h,l} = \frac{\varepsilon_0\varepsilon'}{x_{l,h}}\,\frac{n_{l,h}}{n_f},$$

where $n_{l,h}$ — carrier concentration at the corresponding deep level. Capacitances C_{1-3} describe the bias current in the depletion area, i.e. $C_1 = \varepsilon_0\varepsilon'/x_h$, $C_2 = \varepsilon_0\varepsilon'/(x_l - x_h)$, $C_3 = \varepsilon_0\varepsilon'/(d - x_l)$. Here and below, we consider capacitances and resistances per unit contact area, i.e. in the final expressions for the elements of the equivalent circuit, the area S_a should be introduced. In the scheme in fig. 7 we took into account the resistance of the Schottky contact at direct current R_c, which is absent in [27–30]. For the studied structure, $R_c = 3 \cdot 10^3$ Ohm $\cdot$ cm^2 was obtained from the corresponding measurements at $f = 0$. Using the equivalent circuit of the contact, it is easy to show that the resistance R_c should be taken into account at $f < 1$ MHz, i.e., at frequencies much lower than the minimum frequency $f = 0.1$ GHz for the spectrum $R(f)$ measured in this paper. In the frequency range under consideration, we can assume $R_c \to \infty$. At the same time, for lower frequencies, at which traps with a long recharge time τ_t are studied, the resistance R_c often masks the contribution of traps to the total resistance of the structure with a barrier contact.

The impedance of the structure between points A and B in Fig. 7 is expressed as

$$Z_{AB} = R_{AB} - i\,\frac{1}{\omega C_{AB}}, \qquad (14)$$

where

$$R_{\mathrm{AB}} = \frac{R_h^t (C_h^t)^2/(C_\infty^{\mathrm{AB}})^2}{(1 + C_h^t/C_\infty^{\mathrm{AB}})^2(1+\omega^2\tau_{\mathrm{AB}}^2)}, \qquad (15a)$$

$$C_{\mathrm{AB}} = C_\infty^{\mathrm{AB}} \frac{1+\omega^2\tau_{\mathrm{AB}}^2}{(C_\infty^{\mathrm{AB}}/C_0^{\mathrm{AB}}) + \omega^2\tau_{\mathrm{AB}}^2}. \qquad (15b)$$

Here $C_\infty^{\mathrm{AB}} = C_1$, $C_0^{\mathrm{AB}} = C_\infty^{\mathrm{AB}} + C_h^t$, $\tau_{\mathrm{AB}} = \tau_h/(1+C_h/C_\infty^{\mathrm{AB}})$. According to (15b), the change in the capacitance of $C_{\mathrm{AB}}(\omega)$ under the influence of recharging of *h*-traps occurs between the values $C_{\mathrm{AB}}(\omega \to 0) = C_0^{\mathrm{AB}}$ and $C_{\mathrm{AB}}(\omega \to \infty) = C_\infty^{\mathrm{AB}}$ by C_h^t. Since we did not observe this transition in the measurements of the spectra of $X(f)$ (see Fig. 4, *a* and *c*), we should assume that $C_h^t \ll C_1$ or $n_h/n_f \ll 1$. In such a case we obtain $\tau_{\mathrm{AB}} = \tau_h$, $C_{\mathrm{AB}} = C_1$. Let us take into account that in the approximation of complete depletion we have $x_h = d_0\sqrt{\frac{\Delta_h}{eUc}}$. As a result, we get

$$R_{\mathrm{AB}}(\omega) = R_h(\omega) = \frac{\rho_h}{1+\omega^2\tau_h^2}, \qquad (16)$$

where

$$\rho_h = \frac{\tau_h d_0}{\varepsilon_0\varepsilon'}\sqrt{\frac{\Delta_h}{eU_c}}\,\frac{n_h}{n_f}.$$

Part of the impedance between points A and C, associated with the recharging of *h*-traps, takes the form

$$Z'_{\mathrm{AC}} = -\frac{i}{\omega C_{12}} + R_h(\omega),$$

where

$$C_{12} = \varepsilon_0\varepsilon'/x_l.$$

The next task is to calculate the total impedance Z_{AC} of the parallel connection of the Z_l^t and Z'_{AC}. In the corresponding conversions of the formulas, as well as for *h*-traps, we take into account the relation $C_l^t \ll C_{12}$. Let us note that the effect of *l*-traps on the capacitance spectrum of $C(\omega)$ (unlike *h*-traps) is quite clearly seen in the experiment (curves *1, 2* in Fig. 4, *a* for the $X(f)$ spectra in the $f < 0.5$ GHz range). Nevertheless, this condition is obviously satisfied. Let us take into account the relation

$$\rho_h \ll \rho_l = \frac{\tau_l d_0}{\varepsilon_0\varepsilon'}\sqrt{\frac{\Delta_l}{eU_c}}\,\frac{n_l}{n_f},$$

which is realized in the experimental spectra of $R(f)$ in Fig. 4, *b* and *d*. In these figures, the corresponding parameters, taking into account the contact areas, are the saturation resistances of the functions (16) $R_S^h = R(\tau_l^{-1} < 2\pi f < \tau_h^{-l})$ and $R_S^l = R(2\pi f < \tau_l^{-l})$. Omitting rather cumbersome conversions, we present the final expression for the total impedance of the depletion region:

$$\tilde{Z}(\omega) = Z_{\mathrm{AD}}(\omega) = -\frac{i}{\omega C_3} + Z_{\mathrm{AC}}(\omega)$$

$$= -\frac{i}{\omega C_d} + R_l(\omega) + R_h(\omega), \qquad (17)$$

where the expression for resistance $R_l(\omega)$ is the same as (16) after substitution of indices $h \to l$.

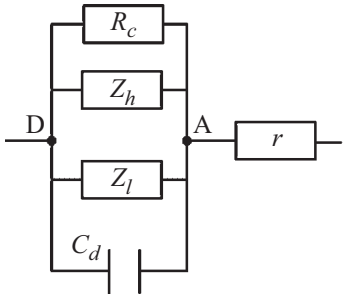

Figure 8. Modified equivalent scheme of the structure. The depletion area is located between points A and D (cf. with Fig. 7).

As a result of the analysis, based on the theory [28], we came to formulas (6), (8), (9) up to the function $\chi_{h,l}(U)$ (10), which describes the dependence of resistance on bias voltage U. In the model considered above, according to the formula (16), together with the obtained expressions for $\rho_{l,h}$ we have $\chi_{h,l}(U) = 1$. Thus, the considered model quite adequately describes our experimental results at $U = 0$. At the same time, the experimental spectra in Fig. 4, *b* and *d* demonstrate a very significant increase in the functions $R(U)$ in the frequency range, where, according to the assumption made, the observed excess resistance is associated with traps recharging. Let us note that at [27,30] developed a somewhat different approach to the analysis of the impedance of a barrier contact with traps. According to these works, the $Z(\omega)$ impedance can be described by a simpler equivalent circuit shown in Fig. 8, where the components of the $R_{l,h}^t, C_{l,h}^t$ trap impedance are given by the above relations and additionally take into account the resistance r of the unperturbed area. Analysis of the corresponding scheme leads to formulas (16), (17), i.e., also gives $\chi_{h,l}(U) = 1$. In the paper [29] for a particular case of shallow traps $\Delta_{l,h} \ll eU_c$, which are also considered in this paper, another expression was obtained for the circuit elements in Fig. 8:

$$C^t = \tau_t/R^t = \frac{\varepsilon_0\varepsilon'}{d}\,\frac{n_t}{n_f}.$$

The difference is in the replacement of $x_t \to d$, as a result of which we have the formula (10), and in the formula (9) $\rho_t = (\tau_t/c_0)(n_t/n_f)$. In this form, the $\chi_t(U)$ function satisfactorily describes the obtained experimental data, at least for *h*-traps (curve *1* in Fig. 6).

5. Conclusion

The method of local microwave $Z-V$ spectroscopy was applied to the study of a layered semiconductor structure in the form of a doped film grown on a conductive substrate. With the lateral resolution 15–30 μm, the main electrophysical parameters of the film are determined — concentration, mobility and type of the free charge carriers, electrical conductivity, bending of the zones near the

boundary with the metal. In the considered situation, the generally accepted four-probe method in the Van der Pauw geometry is not effective due to the shunting action of the substrate. We note the importance of microwave measurements up to frequencies 30–50 GHz to achieve micron resolution. At $a \sim 10\,\mu$m, it is required to measure a very small capacitance of the contact $C \sim 10-50$ fF. As a result, the noise of the spectrometer when measuring the reflectance of the probe leads to significant errors in determining the reactance $X \sim 10^4-10^5$ Ohm in the range $f = 0.01-0.1$ GHz, which can be seen from Fig. 4, *a* and *c*. As the frequency increases, the $X = 1/(\omega C)$ reactance decreases, resulting in an increase in the accuracy of its measurement. Even higher problems arise when determining the resistance $R(f)$ at low frequencies due to the ratio $R \ll X$ (see Fig. 4, *b* and *d*).

The capabilities of the probe station used in the measurements allow in potential to increase the resolution up to $3-5\,\mu$m. The problem of diagnostics with such a resolution may be the detected excess resistance, which will exceed the resistance of the unperturbed region of the semiconductor at high frequencies of the spectrum $f = 20-40$ GHz. The corresponding trend is visible when comparing Fig. 4, *b* and *d*. In this paper, this problem is solved by modeling the excess resistance spectrum using the $R_{l,h}(f)$ functions, the parameters of which are determined at lower frequencies. Possibility of transition to nanometer resolution is not obvious today and requires separate studies. An important task is also the implementation of non-contact measurements. Non-contact nanoscopy of semiconductors is performed using near-field microwave microscopes [7–9,11,13,14]. Despite the optimistic conclusions of these papers, the quantitative characterization of semiconductor materials and structures encounters serious difficulties associated with uncontrolled characteristics of the perturbed near-surface layer of the sample with a complex geometry of microscope probes. Let us once again emphasize the importance of measuring the resistance spectrum $R(f, U)$ along with measuring the reactance $X(f, U)$. The latest measurements, called capacitance-voltage diagnostics, are a classic method for studying semiconductors in order to restore the depth profile of the concentration of free charge carriers ($C-V$ diagnostics). Usually $C-V$ diagnostics is performed at frequencies $f < 1-10$ MHz with a resolution not higher than $0.1-1$ mm. Microwave measurements of the spectrum $Z(f, U)$ ($Z-V$method) provide micron resolution and allow to determine the carrier mobility along with the concentration.

We related the observed features of the resistance spectra $R(f, U)$ to the traps present in the sample. Traps with extremely low recharge time $\tau_h \sim 4 \cdot 10^{-11}$ s, as far as we know, have not previously been observed by direct high-frequency measurements. Nevertheless, the time $\tau_t \sim 10^{-9}-10^{-11}$, the time $\tau_t \sim 10^{-9}-10^{-11}$ s for shallow traps ($\Delta_t \approx 90-100$ meV) was predicted in [29] from indirect measurements in the frequency range $f \sim 100$ kHz at temperatures $T \sim 100$ K. The fact is that the recharge time exponentially increases with decreasing temperature as $\tau_t \sim \exp[\Delta_t/(\kappa T)]$ (κ — Boltzmann's constant). Low-frequency non-local measurements with the temperature pass-through (admittance spectroscopy) are a classic method for studying traps. In this work, the corresponding times were obtained by direct measurements of the high-frequency spectra $R(f)$ at room temperature. Confident measurement of a spectrum similar to $R_h(f)$ is possible in the frequency range $f > 1$ GHz with a contact diameter $a < 50\,\mu$m. At lower frequencies, the resistance R_h of the studied sample is masked by low-frequency traps R_l. However, even in the absence of *l*-traps, the resulting effect could be taken as the resistance r of the unperturbed region of the semiconductor due to saturation of the $R_h(f) \to R_S$ function at $f < 2$ GHz. As the contact diameter a increases, the difference between the r and R_S values of the $R(f)$ function decreases, which can be seen by comparing Fig. 4, *b, d*. At $a > 100\,\mu$m, the indicated difference would be difficult to observe due to the spectrum $R(f)$ noisy. Thus, the developed $Z-V$ method is actually a microwave analogue of admittance spectroscopy, which allows to study high-frequency traps with micron resolution at room temperature. Nevertheless, it would be important to make additional temperature measurements in order to more confidently interpret the observed features of the $R(f, U)$ spectrum.

Acknowledgments

The authors are grateful to S.A. Kraev and E.A. Arkhipova, who made the antenna system for the studied sample; M.N. Drozdov and S.A. Korolev, who performed SIMS and VDP measurements.

Funding

The study has been performed under the scientific program of the National Center for Physics and Mathematics (the „Nuclear and Radiation Physics“ project). The used equipment was provided by the Center of Shared Use of the Institute for Physics of Microstructures RAS (IPM RAS) „Physics and technology of micro- and nano-structures“.

Conflict of interest

The authors declare that they have no conflict of interest.

References

[1] S.M. Anlage, V.V. Talanov, A.R. Schwartz. „*Principles of Near-Field Microwave microscopy*“, *in Scanning Probe Microscopy: Electrical and Electromechanical Phenomena at the Nanoscale,* ed. by S.Kalinin and A. Gruverman (Springer Verlag, Berlin, 2007) p. 215.

[2] K. Lai, W. Kundhikanjana, M.A. Kelly, Z.-X. Shen. Appl. Nanosci., **1**, 13 (2011).

[3] A. Imtiaz, T.M. Wallis, P. Kabos. IEEE Micrwave Mag., **15**, 52 (2014).

[4] S. Berweger, T.M. Wallis, P. Kabos. IEEE Micrwave Mag., **21**, 36 (2020).
[5] A.N. Reznik, E.V. Demidov. J. Appl. Phys., **113**, 094501 (2013).
[6] A.N. Reznik, S.A. Korolyov. J. Appl. Phys., **119**, 094504 (2016).
[7] O. Amster, F. Stanke, S. Friedman, Y. Yang, St.J. Dixon-Warren, B. Drevniok. Microelectron. Reliab., **76–77**, 214 (2017).
[8] S. Hommel, N. Killat, A. Altes, T. Schweinboeck, F. Kreupl. Microelectron. Reliab., **76–77**, 221 (2017).
[9] S. Berweger, G.A. MacDonald, M. Yang, K.J. Coakley, J.J. Berry, K. Zhu, F.W. DelRio, T.M. Wallis, P. Kabos. Nano Lett., **17**, 1796 (2017).
[10] A.N. Reznik, S.A. Korolyov, M.N. Drozdov. J. Appl. Phys., **121**, 164503 (2017).
[11] A. Buchter, J. Hoffman, A. Delvallee, E. Brinciotti, D. Hapiuk, C. Licitra, K. Louarn, A. Arnoult, G. Almuneau, F. Piquemal, M. Zeier, F. Kienberger. Rev. Sci. Instrum., **89**, 023704 (2018).
[12] S.A. Korolyov, A.N. Reznik. Rev. Sci. Instrum., **89**, 023706 (2018).
[13] X. Guo, K. Bertling, A.D. Rakic. Appl. Phys. Lett., **118**, 041103 (2021).
[14] X. Guo, X. He, Z. Degnan, B.C. Donose, K. Bertling, A. Fedorov, A.D. Rakic, P. Jacobson. Appl. Phys. Lett., **119**, 091101 (2021).
[15] V.L. Bonch-Bruevich, S.G. Kalashnikov. *Physics of Semiconductors* (VEB, Berlin, 1982).
[16] A.N. Reznik, N.V. Vostokov, N.K. Vdovicheva, S.A. Korolyov, V.I. Shashkin. J. Appl. Phys., **122**, 244505 (2017).
[17] A.N. Reznik, N.V. Vostokov, N.K. Vdovicheva, V.I. Shashkin. Techn. Phys., **64** (11), 1859 (2020).
[18] A.N. Reznik, N.K. Vdovicheva. Techn. Phys., **64** (11), 1722 (2019).
[19] A.N. Reznik, N.V. Vostokov. Techn. Phys., **92** (3), 408 (2022).
[20] S.M. Sze, K.K. Ng. *Physics of Semiconductor Devices* (John Wiley & Sons, Inc., 2007).
[21] L.E. Dickens. IEEE Trans. Microwave Theory Techn., **15**, 101 (1967).
[22] J.H. Lee, S. Huyn, K. Char. Rev. Sci. Instrum., **72**, 1425 (2001).
[23] M. Golosovsky, E. Maniv, D. Davidov, A. Frenkel. IEEE Trans. Instrum. Measur., **51**, 1090 (2001).
[24] S. Hoshina, Y. Kanai, M. Miyakawa. IEEE Trans. Magn., **37**, 3311 (2001).
[25] D.D. Hagl, D. Popovic, S.C. Hagness, J.H. Booske, M. Okonevwski. IEEE Trans. Microwave Theory Techn., **51**, 1194 (2003).
[26] M.A. Galin, A.N. Reznik. J. Commun. Technol. Electron., **54** (3), 259 (2009).
[27] W.G. Oldham, S.S. Naik. Solid-State Electron., **15**, 1085 (1972).
[28] M. Beguwala, C.R. Crwell. Solid-State Electron., **17**, 203 (1974).
[29] G. Vincent, D. Bois, P. Pinard. J. Appl. Phys., **46**, 5173 (1975).
[30] J.L. Pautrat, B. Katirciogly, N. Magnea, D. Bensahel, J.C. Pfister, L. Revoil. Solid-State Electron., **23**, 1159 (1980).

Translated by E.Potapova